Flow of polar and nonpolar liquids through nanotubes: A computational study

Andrii Kyrylchuk [1,2] and David Tománek [1,*]

[1] *Physics and Astronomy Department, Michigan State University, East Lansing, Michigan 48824-2320, USA*

[2] *Institute of Organic Chemistry, National Academy of Sciences of Ukraine, Murmanska Street 5, 02660 Kyiv, Ukraine*

(Received 30 May 2020; revised 23 May 2021; accepted 28 June 2021; published 26 July 2021)

We perform *ab initio* density functional calculations to study the flow of water, methanol, and dimethyl ether through nanotubes of carbon and boron nitride with different diameters and chiralities. The liquids we choose are important solvents, with water and methanol being polar and dimethyl ether being nonpolar. In terms of activation barriers for liquid transport, we find the molecular-level drag to decrease with decreasing nanotube diameter but to be rather independent of the chiral index. We also find molecules with higher polarity to generally experience higher drag during flow. Counterintuitively, we find the drag for water in boron nitride nanotubes not to exceed that in carbon nanotubes due to frustration in competing long-range Coulomb interactions.

DOI: 10.1103/PhysRevMaterials.5.076001

I. INTRODUCTION

The field of micro- and nanofluidics has been evolving rapidly during the last decades, with its broad impact ranging from medical devices [1–3] to advanced fabrics and energy conversion devices [4–6] and advanced membranes for water desalination by reverse osmosis [7]. Aligned carbon nanotube (CNT) membranes attract much interest because of their well-defined pore size, their capability to form composite matrices [8], and their resistance to biofouling [9]. Many useful properties of CNTs are also found in related boron nitride (BN) nanotubes (BNNTs) formed of hexagonal boron nitride [10]. These benefits, combined with high thermal, chemical, and mechanical stability, should make CNTs and BNNTs very suitable materials to form membranes [8]. Consequently, understanding the flow of fluids inside nanometer-sized channels in these nanotubes is of growing importance [11].

Since liquid flow inside nanotubes could not be observed with subnanometer resolution so far, our understanding to date has relied almost exclusively on molecular dynamics (MD) simulations. Many force fields have been developed to describe the delicate interplay among the strong and weak forces that determine the behavior of liquids including water [6,12–16], but none has been able to satisfactorily reproduce all aspects of their behavior including their interaction with solids in an unbiased manner. Such calculations provide valuable information, but final results depend heavily on models used for interatomic interactions, including the flexibility of bond lengths and angles in water, molecular polarizability, and long-range electrostatic interactions [6,16]. On the other hand, force fields based on *ab initio* total energy functionals including density functional theory (DFT) are nominally free of adjustable parameters, but high computational requirements have severely limited their use.

Much insight has been obtained so far using MD simulations. Occurrence of water wires inside small CNTs has been revealed by model force field simulations [12–15]. These results were confirmed by *ab initio* DFT calculations [17,18] and Raman spectroscopy observations [19]. Formation of stacked ring structures in wide CNTs with diameters $\gtrsim$10 Å has been corroborated by MD simulations based on model force fields [14,20–22] and DFT [23]. These findings were experimentally confirmed by infrared (IR) spectroscopy [24] and x-ray diffraction [25].

Still, many open questions remain [11] in relationship to mass transport of liquids through nanotubes and nanopores in general. Some experimental evidence [26–30] even suggests that the flow velocity of liquids inside nanometer-sized pores is several orders of magnitude higher than what conventional theory based on Newtonian flow and the Hagen-Poiseuille equation would predict [31]. There are clearly some pitfalls in the way to translate and interpret experimental data into microscopic fluid flow speeds [7]. In particular, slip-flow of liquids inside nanochannels of different types needs to be addressed. To date, there are no conclusive experimental or parameter-free *ab initio* results regarding the dependence of fluid flow inside nanotubes in terms of nanotube type and composition, diameter, and chirality.

In this paper we address atomic-scale details of the flow of water, methanol, and dimethyl ether through nanotubes of carbon and boron nitride with different diameters and chiralities. These liquids are important solvents, with water and methanol being polar and dimethyl ether being nonpolar. We determine the potential energy of isolated molecules along the inner nanotube surface to obtain activation barriers for diffusion, which translate into molecular-level drag. We find this drag to decrease with decreasing nanotube diameter but to be rather independent of the chiral index. We also find that molecules with higher polarity generally experience higher drag during flow.

II. COMPUTATIONAL APPROACH

Our computational approach to study liquid water and other solvents interacting with carbon nanotubes is based on

*tomanek@msu.edu

ab initio DFT as implemented in the Spanish initiative for electronic simulations with thousands of atoms (SIESTA) [32] code. These results were compared with those based on the Vienna *ab initio* simulation package (VASP) [33–36] code. Unless specified otherwise, we used the nonlocal Perdew-Burke-Ernzerhof (PBE) [37] exchange-correlation functional in SIESTA, norm-conserving Troullier-Martins pseudopotentials [38], a double-ζ basis including polarization orbitals, and a mesh cutoff energy of 500 Ry to determine the self-consistent charge density. For selected systems, our PBE results were compared with those obtained using the optimized van der Waals hybrid functional vdW-optB86b [39,40]. We have used periodic boundary conditions throughout the study, with nanotubes separated by $\gtrsim$9 Å vacuum space. The nanotube segments were either primitive unit cells or supercells that were >15 Å long to suppress interaction between replicas of the enclosed molecules, and the reciprocal space was sampled by a uniform $1 \times 1 \times 2$ k-point grid [41]. Further increase in the k-point density had no effect on the energy. Systems with unit cells longer than >30 Å have been represented by the Γ point only. This provided us with a precision in binding energy of $\lesssim$2 meV/atom with respect to isolated atoms. Geometries have been optimized using the conjugate gradient (CG) method [42], until none of the residual Hellmann-Feynman forces exceeded 10^{-2} eV/Å. While computationally rather demanding, the DFT-PBE energy functional is free of adjustable parameters and has been used extensively to provide an unbiased description of water and its interaction with solids [23,43].

Selected MD simulations were performed to study the dynamics of water inside carbon nanotubes. We found that 0.3-fs time steps were sufficiently short to guarantee energy conservation in a microcanonical ensemble. The flow of water induced by a pressure difference between the tube ends was described using an approach developed earlier [7].

III. RESULTS

As mentioned above, the vast majority of atomistic MD simulations are based on parametrized force fields, which offer a high degree of numerical efficiency and allow one to study the motion of several thousand atoms simultaneously. The drawback of this approach is its lack of universality and quantitative predictability: Force fields optimized for bulk fluids need to be changed at interfaces and in situations where long-range electrostatic interactions play a role [6,16]. For this reason, we decided to use the *ab initio* DFT formalism in our study. In spite of its high computational demand, DFT is nominally free of parameters and independent of predefined assumptions. This approach has been validated in successfully predicting static and dynamic properties of liquid water [7] and should provide valuable information that should complement large-scale studies with parametrized force fields.

We recall that in microcanonical MD simulations, the total energy remains constant, but the potential energy and the kinetic energy (which corresponds to the instant temperature) change with time. These fluctuations are finite in systems with a finite number of atoms N (in the unit cell) and only vanish for $N \to \infty$. Statistical fluctuations limit the accuracy of the expectation value of the potential energy. Thus MD simulations are of limited value when studying potential energy surfaces for the diffusion process.

To obtain accurate potential energy surfaces for molecular diffusion, the following results are obtained using static calculations rather than MD simulations. As a good indication of the drag, which molecules experience at the interface during flow through narrow cavities, we calculated the potential energy of a single molecule drifting along nanotubes with different compositions, diameters, and chiral indices. These results reveal potential energy barriers that should correlate with the friction coefficients and slip lengths. We oriented the nanotube axis along the z direction and fixed all nanotube atoms in their relaxed positions. We then determined the interaction energy between the enclosed molecule M and the nanotube, defined by

$$E = E_{\rm tot}(M@NT) - E_{\rm tot}(M) - E_{\rm tot}(NT). \quad (1)$$

A negative value of E indicates an energetic preference for M to be inside rather than to be isolated from the nanotube. In this paper, the position of a molecule along the z axis of a nanotube is given by the z coordinate of one representative atom. For an N-atom molecule, the remaining $3N-1$ degrees of freedom are globally optimized to provide the energy $E(z)$. The optimization process typically starts close to the inner nanotube surface and leaves the molecule free to find its optimum position within the x-y plane normal to the tube axis and to optimize its shape and orientation. We considered a result to be converged when the same final geometry with the same energy was reached from different starting positions. The full $E(z)$ potential energy surface along the nanotube was obtained using a sequence of z values. For each system of interest, we chose a sufficiently dense z-value grid to represent the potential energy surface accurately. Specific z values used are indicated by the data points in Figs. 2–6.

A. Water interactions with CNTs

Our first study was dedicated to the interaction of individual water molecules with a CNT and a BNNT. The position of the H_2O molecule along the tube axis, which is parallel to the z axis, is represented the z coordinate of the oxygen atom. "Snapshots" of a water molecule inside the (12,6) CNT and BNNT are shown in Fig. 1.

Quantitative results for $E(z)$ for water inside an armchair (8,8) and a zigzag (14,0) CNT with essentially the same diameter $d = 11.0$ Å are presented in Fig. 2. We have optimized the H_2O molecule using two starting configurations, with the CNT inner wall facing either the H atoms (H_2O-H/CNT) or facing the oxygen (H_2O-O/CNT). Chemical intuition suggests a repulsion between the oxygen lone electron pairs and the π system of the CNT, pushing the molecule toward the center. The small positive charge on the hydrogen atoms, on the other hand, should attract the molecule towards the wall. This is confirmed by our results in Fig. 2(a): A water molecule gains $\lesssim$98.9 meV when entering an armchair (8,8) CNT with oxygen facing the wall and as much as $\approx$157.3 meV when the hydrogens face the wall. Of these two configurations, the

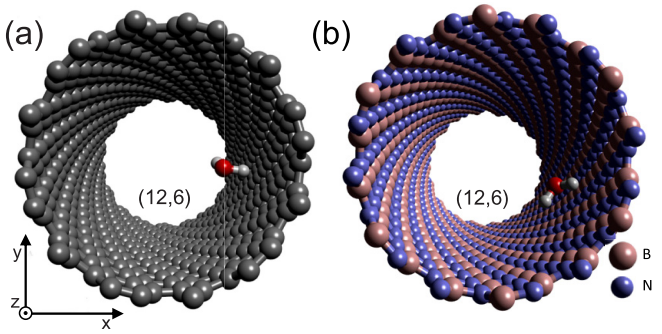

FIG. 1. A (12,6) chiral nanotube of (a) carbon and (b) boron nitride (BN), containing one water molecule.

one with oxygen facing the wall is metastable. As seen in Fig. 2(b), we find roughly the same binding energies for the two configurations in the zigzag (14,0) CNT with the same diameter.

The weaker interaction in the metastable configuration with O facing the wall also results in a very weak dependence of $E(z)$ on the position of the molecule both in the (8,8) and in the (14,0) CNT. In this orientation, H_2O may slip along the CNT wall with essentially no barrier. The situation is different in the stable configuration of water facing the CNT wall with its hydrogen atoms. Besides a higher binding energy in this orientation, also the barriers in $E(z)$ are significantly higher, of the order of 40 meV. The precise position of the minima and maxima results from the hydrogen pair in H_2O finding a match or a mismatch with C atoms in the graphitic CNT wall. Especially in wide CNTs, the range of $E(z)$ values is approximately the same, independent of chirality, since it essentially represents the interaction of a water molecule with a graphene layer. It is only the sequence of minima and maxima that distinguishes between chiral indices in the same way as different sequences of maxima and minima occur when a water molecule crosses a graphene sheet along different trajectories.

In the following investigations, we will only consider the stable configuration of H_2O molecules facing the nanotube wall with their hydrogen atoms.

B. Water diffusion inside zigzag and armchair CNTs

We display the potential energy surface $E(z)$ for water diffusion inside CNTs with selected chiral indices in Fig. 3. A more complete list of potential energy barriers E_p is presented in Table I. As a general trend, we notice that the size of the diffusion barriers decreases with decreasing CNT diameter. We also find that the H_2O-CNT interaction increases with decreasing nanotube diameter, making narrower CNTs more hydrophilic. Thus, with decreasing tube diameter d, CNTs first turn from hydrophobic ($d\to\infty$ for graphene) to increasingly hydrophilic. Eventually, they turn hydrophobic again at diameters too small to accommodate a water molecule. The increase in the H_2O-CNT interaction and reduction of activation barriers is linked to the fact that in very narrow nanotubes, atoms all around the nanotube perimeter interact with the enclosed molecule. While stabilizing the enclosed molecule, it results in frustrated geometries that reduce the dependence of the interaction energy E on the position of the molecule z. This general trend has already been identified in published MD simulations based on parametrized force fields [44,45]. In agreement with our findings, these studies found that slip lengths of water molecules decreased with increasing CNT diameter and asymptotically approached the value for water on planar graphene.

The presented quantitative findings compare well with published DFT-PBE results for the drift of a monolayer of two-dimensional (2D) ice on graphene, suggesting energy barriers of ≈15 meV/H_2O along the zigzag and ≈25 meV/H_2O along the armchair direction [46]. We note that the strong H_2O-H_2O interaction in ice does not alow individual water

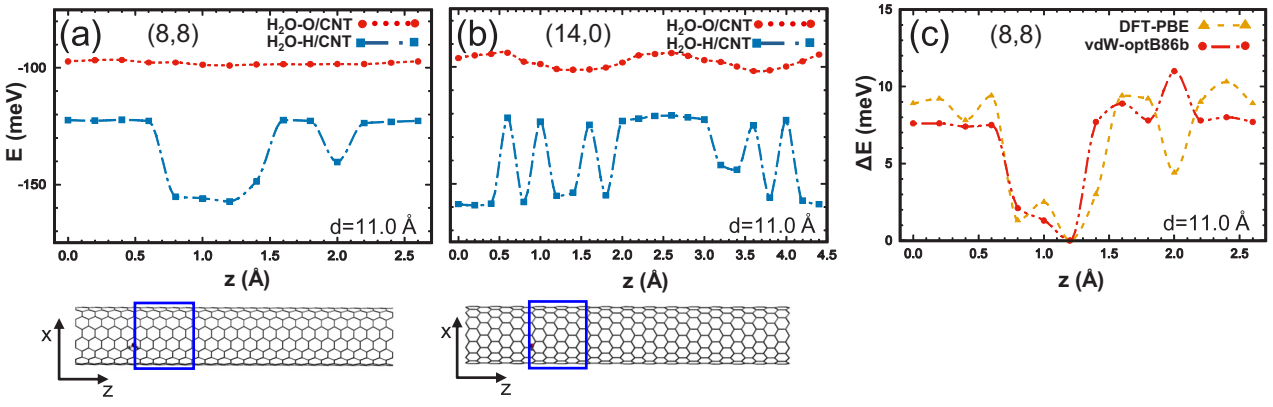

FIG. 2. Interaction energy $E(z)$ between an isolated H_2O molecule and a surrounding (a) armchair (8,8) and (b) zigzag (14,0) CNT obtained using the SIESTA code. The range of $E(z)$ values is the same in (a) and (b). We distinguish the H_2O-H/CNT configuration, where the H end of H_2O faces the wall, from H_2O-O/CNT, where the O end faces the wall. Negative values of E indicate energetic preference for H_2O entering the nanotube. The lower panels give a schematic view of the respective nanotubes. The size of the unit cell considered is outlined by the blue box. (c) Comparison between energy changes $\Delta E(z) = E(z) - E_{\min}$ along the trajectory in (a) obtained using the DFT-PBE and the vdW-optB86b energy functionals in the VASP code. Nanotube diameters d are indicated in the individual panels. The z coordinate represents the water position along the z axis of the CNT.

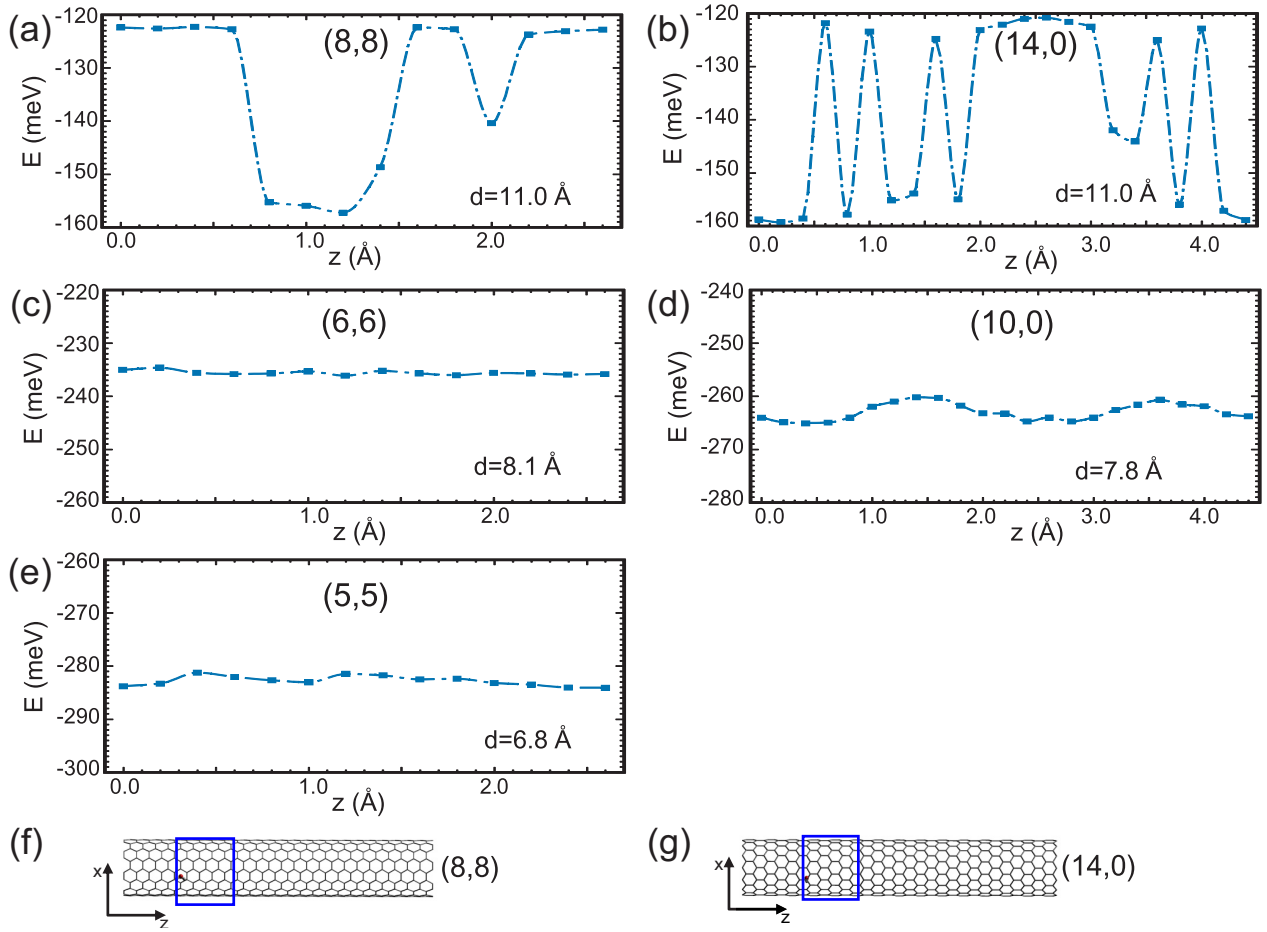

FIG. 3. Interaction energy $E(z)$ between an isolated H_2O molecule and a surrounding (a) (8,8), (b) (14,0), (c) (6,6), (d) (10,0), and (e) (5,5) CNT. The z coordinate represents the water position along the z axis of the CNT. Only the stable water orientation with the hydrogens facing the wall is considered. The range of $E(z)$ values is 40 meV in all panels. Schematic geometry is shown for (f) the (8,8) and (g) the (14,0) CNT, with the size of the unit cell considered being outlined by the blue box. Nanotube diameters d are indicated in the individual panels.

molecules the same configurational freedom as the geometry considered here.

Our results in Table I also suggest that potential energy barriers E_p in zigzag CNTs are typically higher by ≈3 meV than in armchair nanotubes. At this point, we should realize that drift occurs along the armchair direction in CNTs with a zigzag edge and along the zigzag direction in nanotubes with an armchair edge. Even though the small difference between activation barriers approaches the precision limit of DFT-PBE, we are pleased that our results for a single H_2O molecule match those for 2D ice/graphene [46] quite well. A similar small difference between activation barriers in zigzag and armchair nanotubes, based on MD simulations with parametrized force fields, has been reported previously [47,48].

TABLE I. Energy barriers E_p for the diffusion of an isolated H_2O molecule along CNTs with a specific chiral index and diameter d. Reported results are for orientation of the molecule with its hydrogen pair facing the wall.

Chiral index	d (Å)	E_p (meV)
(5,5)	6.8	2.8
(6,6)	8.1	1.5
(10,0)	7.8	4.9
(8,8)	11.0	35.0
(14,0)	11.0	38.5
(10,6)	11.0	37.6
(11,5)	11.1	36.5
(12,3)	10.8	37.3

We noted another point of interest when studying the passage of a water molecule through a very narrow (5,5) nanotube. Considering the van der Waals diameter $d_{vdW}(H_2O) = 2.8$ Å of a water molecule [49] and the van der Waals radius $r_{vdW}(C_{atom}) = 1.8$ Å [50] of a carbon atom, the sum $d_{vdW}(H_2O) + 2r_{vdW}(C_{atom}) = 6.4$ Å is only 0.5 Å smaller than the diameter $d = 6.9$ Å of the (5,5) CNT. In other words, this is a rather tight fit for the enclosed molecule. Naïvely, pressing the molecule against the wall should increase the activation barrier for diffusion. In reality, the opposite is true. The molecule now interacts with many atoms along the perimeter of the surrounding nanotube, with unfavorable interactions compensating favorable interactions in different regions. The resulting frustration lowers the activation barriers for diffusion.

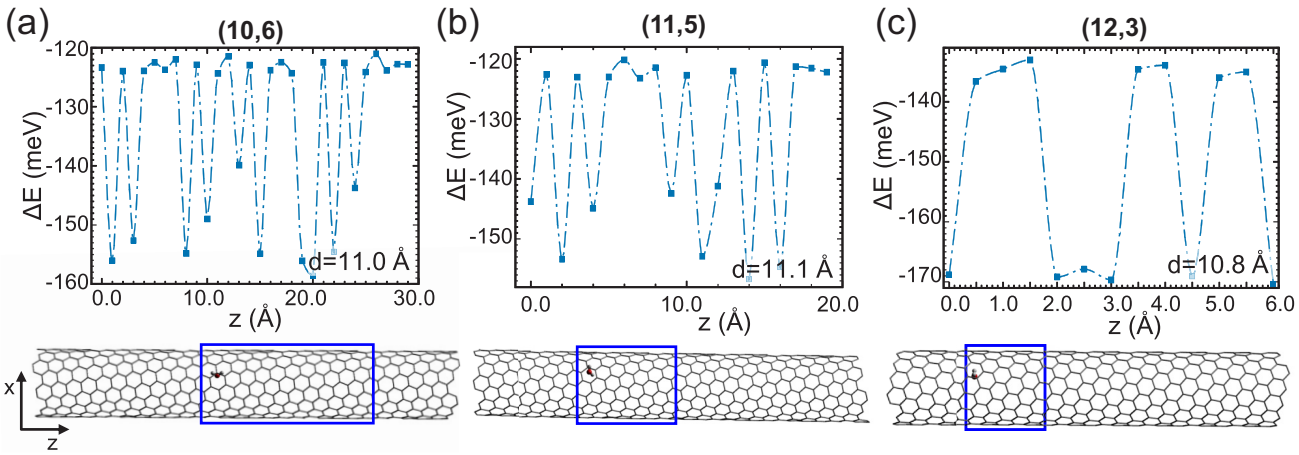

FIG. 4. Interaction energy $E(z)$ between an isolated H_2O molecule and a surrounding (a) (10,6), (b) (11,5), and (c) (12,3) CNT. The range of $E(z)$ values is 40 meV in all panels. Nanotube diameters d are indicated in the individual panels. The z coordinate represents the water position along the z axis of the CNT. Only the stable water orientation with the hydrogens facing the wall is considered. Schematic geometries including the unit cells considered are shown below the respective $E(z)$ plots.

C. Water diffusion inside chiral CNTs

To complete our study of water in CNTs, we present $E(z)$ results for water inside three chiral nanotubes with a similar diameter $d \approx 11$ Å in Fig. 4. We used different z grids to accurately sample different unit cells with their length depending on the chiral index. Our findings of essentially the same energy barrier values $E_p \approx 30$ meV fall in line with all our other results, suggesting that the energy barriers depend primarily on the nanotube diameter, with only minor dependence on the chiral index.

We have also filled the chiral (12,6) CNT with water and used a DFT-PBE-based MD simulation to study the flow driven by the pressure difference between the tube ends, which is counterbalanced by drag. Using a computational approach developed earlier [7], we subjected all H atoms to the force $F = 2.5 \times 10^{-2}$ eV/Å and all O atoms to the force $F = 4.0 \times 10^{-1}$ eV/Å in the axial direction of the nanotube. As seen in Video 1, the nonvanishing chirality of the surrounding CNT does not exert a sufficient torque on the water column to induce axial rotation.

D. Water diffusion inside BNNTs

Similar to graphite, hexagonal boron nitride (h-BN) is a layered material capable of forming nanotubes [10]. Even though h-BN is isoelectronic to graphene, B-N bonds are slightly longer than C-C bonds in graphene. There is a corresponding ≈2% increase in the diameter of BNNTs over CNTs with the same chiral index. Unlike CNTs, all BNNTs are wide-gap insulators. The polar nature of the B-N bond provides additional attraction to polar molecules such as water. In analogy to our CNT results, we present the interaction energy of a water molecule with surrounding (8,8) and (14,0) BNNTs in Fig. 5.

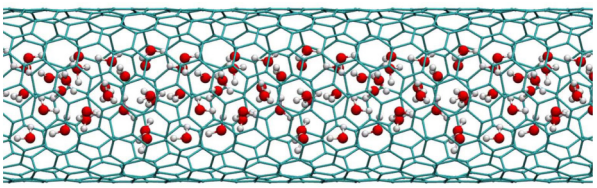

VIDEO 1. MD simulation of water flow through a chiral (12,6) CNT.

Unlike in CNTs of similar diameter, we found optimization of water inside BNNTs to be rather challenging due to a more complex potential energy surface. We believe that the added complexity stems from the long-range nature of the Coulomb interactions, which are important in BNNTs. While we could not guarantee identifying the lowest energy state among many optima with similar energies, our results in Fig. 5 provide consistent trends. For the sake of comparison with the corresponding CNTs, we summed up the van der Waals radii $r_{vdW}(N) = 1.55$ Å of nitrogen [50] and $r_{vdW}(B) = 1.92$ Å of boron [51] and the van der Waals diameter $d_{vdW}(H_2O) = 2.8$ Å of a water molecule [49]. The corresponding diameter of a BNNT that would contain water in a tight fit is 6.3 Å. This value is significantly smaller than the diameter $d \approx 11$ Å of (8,8) and (14,0) BNNTs, indicating that—similar to CNTs—the water molecule is not sterically constrained in these nanotubes.

The suggested additional attraction of water to walls of BNNTs in comparison to CNTs is best illustrated by comparing the E values for H_2O in (8,8) and (14,0) nanotubes of carbon and BN presented in Figs. 3(a) and 3(b) and Fig. 5. For both chiral indices, we see a significant stabilization of water molecules in BNNTs by ≈40 meV over CNTs. A naïve expectation of corresponding increase in activation barriers for diffusion has not materialized; we find a similar value $E_p \approx 40$ meV in all these nanotubes.

The similarity of the activation barriers for water in BNNTs and CNTs has an interesting physical origin. Net charges do not play a major role in the nonpolar bond between H_2O and a CNT, with hydrogens facing the wall, which is

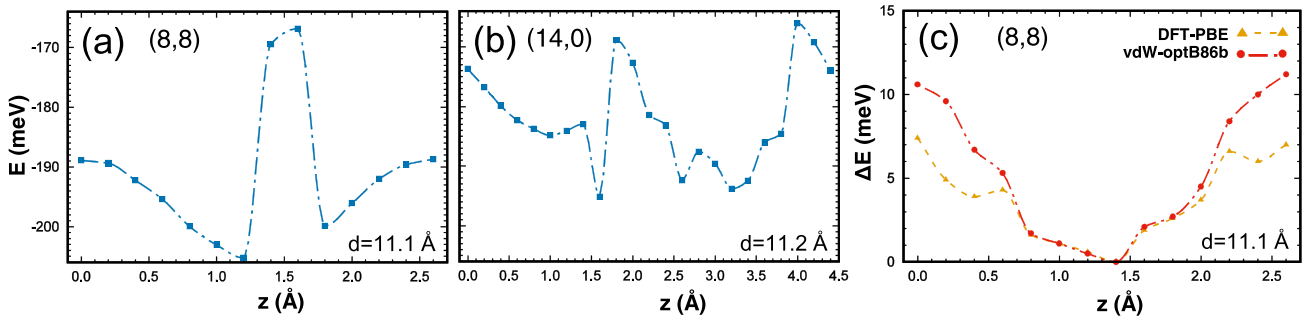

FIG. 5. Interaction energy $E(z)$ between an isolated water molecule contained in an (a) (8,8) and (b) (14,0) BNNT, obtained using the SIESTA code. Nanotube diameters d are indicated in the individual panels. The range of $E(z)$ values is the same in (a) and (b). (c) Comparison between energy changes $\Delta E(z) = E(z) - E_{\min}$ along the trajectory in (a) obtained using the DFT-PBE and the vdW-optB86b energy functionals in the VASP code. The z coordinate represents the position of the molecule along the z axis of the BNNT.

rather local. The situation is rather different for water inside a BNNT. The Coulomb interaction between the polar H_2O molecule is long ranged, involving charges on B and N sites all around the BNNT diameter. Whereas the water dipole encounters a net stabilization inside a BNNT, the competition between significant attractive and repulsive forces that are long ranged leads to a degree of frustration that decreases the dependence of E on the axial position of the molecule.

Controversial results have been reported on water flow through CNTs and BNNTs. Results claiming a faster flow of water in BNNTs than in CNTs [52,53] directly contradict results claiming the opposite [47,54,55].

Setting aside an additional issue of different entry barriers for water in CNTs and BNNTs [56], calculation of diffusion barriers for drifting water, which depend on local orbital hybridization with nanotube atoms as well as long-range Coulomb forces, requires an adequate formalism. The potential energy surface $E(z)$ cannot be reproduced accurately by parametrized short-range potentials [57–59] that ignore long-range Coulomb interactions and tend to exaggerate the value of E_p in BNNTs.

Unlike inside a cylindrical BNNT, there is much less frustration in terms of competing attractive and repulsive forces on planar h-BN. As evidenced by *ab initio* DFT calculations [60], this leads to an increased modulation of E across the h-BN surface in comparison to graphene.

E. Diffusion of different molecules inside CNTs

The above-mentioned application of CNTs for the filtration of water can be trivially extended to other liquids. For a limited number of such liquids there are published experimental and theoretical results [11,29,61–63]. Besides water, we studied methanol (CH_3-OH, Me-OH) and dimethyl ether (CH_3-O-CH_3, MeOMe) molecules that are comparable in size. All three substances are important solvents, with the dielectric constant decreasing from H_2O, to Me-OH, and to MeOMe, as represented in Table II. We studied the potential energy surface $E(z)$ for each of these molecules drifting along the (8,8) CNT in much the same way as described for water earlier. Our results for $E(z)$ are displayed in Fig. 6 and for the energy barriers E_p in Table II.

Sequential substitution of hydrogen atoms by methyl groups substantially lowers the dipole moment p of the molecule and the dielectric constant ϵ of the liquid. This lowers the interaction of the molecule with the inner CNT wall and also the diffusion barriers, as seen clearly by comparing our results for H_2O and methanol in Fig. 6. As seen in Fig. 6(c), this trend is not completely followed by dimethyl ether with a very low static dipole moment.

Whereas increasing the number of hydrogens substituted by methyl groups lowers the dipole moment, the concurrent growth of molecular size increases the molecular polarizability α, reaching its maximum in dimethyl ether. It may be argued that higher values of α correlate with higher reactivity and stronger interaction with the tube wall. In comparison to water, we see a similar bonding enhancement, indicated by lower values of E, in both methanol and dimethyl ether. Our results suggest that increase in either p or α tends to increase the activation barriers for diffusion, which are largest for water and dimethyl ether. In these considerations, we should note that the dielectric constant of a bulk liquid does not fully represent a nanoconfined liquid, where the reorientation process can be constrained. In general, we find changes in the barrier size to be rather modest for the solvents we consider.

IV. DISCUSSION

Most of our calculations focused on a single molecule drifting along a CNT or a BNNT. Even though this geometry is different from a nanotube filled with many molecules

TABLE II. Bulk dielectric constant ϵ, molecular polarizability α, and energy barrier E_p for the diffusion of an isolated solvent molecule inside an (8,8) armchair CNT.

Solvent	Dielectric constant ϵ	Polarizability α [64] ($\times 10^{-24}$ cm^3)	E_p (meV)
Water	80.1	1.45	35.0
Methanol	33.0	3.23···3.32	6.9
Dimethyl ether	6.2	5.16···5.84	12.6

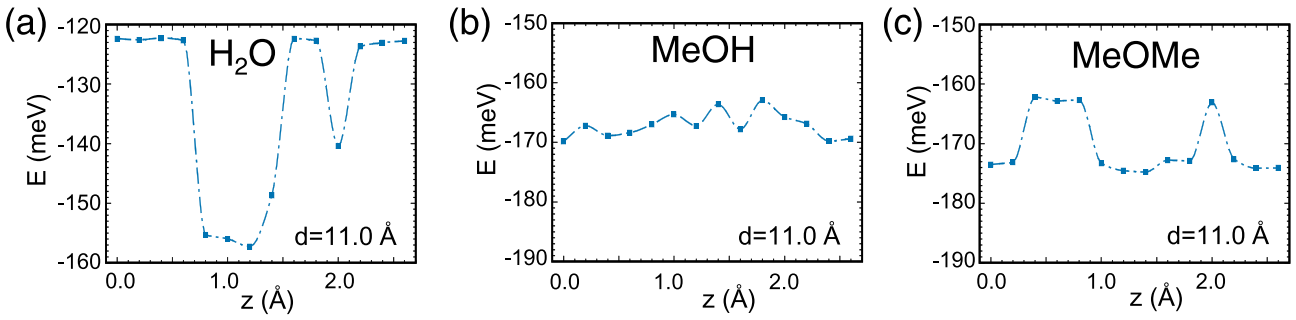

FIG. 6. Interaction energy $E(z)$ between an isolated (a) water (H_2O), (b) methanol (CH_3-OH, MeOH), and (c) dimethyl ether (CH_3-O-CH_3, MeOMe) molecule and a surrounding (8,8) CNT. The range of $E(z)$ values is 40 meV, and nanotube diameters d are indicated in all panels. The z coordinate represents the position of the molecule along the z axis of the CNT.

representing a liquid, a relation between molecular diffusion barriers and the resulting drag force in the liquid has been identified previously [47]. The specific claim, based on MD simulation results for (8,8) and (14,0) CNTs that contain a single H_2O molecule or are filled with water, is that the trends in the friction coefficients are the same in the two cases [47]. Similar to our findings, consistently higher friction coefficients were reported [47] in the zigzag (14,0) CNT than in the armchair (8,8) CNT, which contained either a single H_2O molecule or were filled with water. The friction coefficients in the different CNTs were very close in the single-molecule case and increased in size with increasing water filling level.

We should reiterate that the quasi one-dimensional potential energy surface $E(z)$ reported in Figs. 2–6 is the result of many multidimensional structure optimization studies of molecules contained in unit cells containing typically hundreds of atoms. With only the z position of one atom fixed, the global energy minimum $E(z)$ has to be determined for each data point representing an N-atom molecule in its $(3N-1)$-dimensional configurational space. With molecules containing 3–7 atoms in our study, the molecular configuration spaces are 8–20 dimensional. There is no guaranteed way to find the global minimum in that case, especially at the high computational cost of DFT.

As we discuss in the following, activation barriers determined for an isolated molecule represent the upper limit of potential energy changes per molecule in nanotubes filled with a liquid. Low compressibility and high packing inside the rigid nanotube walls significantly constrain the freedom of each molecule to relax its position to its optimum registry, shape, and orientation. Since the bonding of molecules adjacent to the wall is reduced due to their frustrated configuration, their potential energy surface $E(z)$ is significantly flattened in comparison to single-molecule results. This is also true for vacancy defects that should not hinder the axial drift of molecules [65]. In wide enough nanotubes, $E(z)$ becomes flat for molecules not adjacent to the walls. Using our single-molecule results, these considerations allow us to estimate the range of $\Delta E(z)$ values causing drag of the liquid column in a liquid-filled nanotube during its pluglike motion [66]. The viscosity of the liquid—unlike the friction coefficient—does not contribute much to the drag [67]. To a small degree, the flexibility of the nanotube walls has been shown to further reduce the friction coefficient in comparison to a rigid wall [68,69]. All these considerations are important to correctly estimate $\Delta E(z)$ for a liquid column moving along the tube axis in a way that does not suffer from limitations of MD simulations with finite unit cells.

We observe that barriers for the activated diffusion of MeOH along the CNT wall, reported in Fig. 6, do not lie in between those of polar H_2O and nonpolar MeOMe. Even though a methanol molecule has only one hydrogen bonded directly to an oxygen atom, its properties are rather different from those of a water molecule. The methyl group accounts for almost half of the molecular weight of MeOH, which should double its polarizability and significantly lower its bulk dielectric constant when compared with H_2O. On the other hand, its larger size increases the number of atoms in the nanotube wall that are in direct contact with it. The two opposing effects should modify the corresponding $E(z)$ potential energy surface in comparison to water, possibly explaining the apparent controversy.

The calculated relative barriers for the passage of water and other solvents show that nanotubes and membranes of carbon or BN can indeed be used for the separation of liquids and water purification including desalination [7,8]. Viable applications of membranes containing aligned CNTs may then extend from removal of organic components from water to the purification of gasoline and other petroleum fractions [63]. The former is an especially pressing issue, since state-of-the-art polymer membranes used in the reverse osmosis process are easily destroyed by hydrocarbons [70]. Polymer membranes also have insufficient selectivity to noncharged organic molecules [71] and are prone to biofouling [72–74].

V. SUMMARY AND CONCLUSIONS

We have conducted *ab initio* DFT studies of the drift of water, methanol, and dimethyl ether molecules inside nanotubes of carbon and boron nitride with different diameters and chiral indices. The liquids we choose are important solvents, with water and methanol being polar and dimethyl ether being nonpolar. In terms of activation barriers for transport, we find the molecular-level drag to decrease with decreasing nanotube diameter but to be rather independent of the chiral index. We also found molecules with higher polarity or polarization to experience higher drag during the flow. Rather counterintuitively, we found the drag for water molecules in boron

nitride molecules not to exceed that in carbon nanotubes due to frustration in competing long-range Coulomb interactions. We expect that the trends identified in this paper may help to design nanotube membranes for the filtration of water and separation of solvents.

ACKNOWLEDGMENTS

We thank Aleksandr Noy for valuable discussions and Dan Liu for assistance with VASP calculations. A.K. acknowledges financial support from the Fulbright program. Computational resources for this study have been provided by the Michigan State University High Performance Computing Center.

APPENDIX: EFFECT OF EXCHANGE-CORRELATION FUNCTIONALS ON ENERGIES

Significant effort has been spent recently to correctly describe bonding in noncovalently bonded systems, including weakly bonded layered systems and liquid water. Many exchange-correlation (XC) functionals have been proposed to improve the accuracy of DFT results with respect to quantum-chemical wave-function theory (WFT) approaches. The objective has been to improve the accuracy of binding energies and to adjust Kohn-Sham eigenvalues to match quasiparticle spectra observed in spectroscopy. So far, only one functional we know of, namely, the local density approximation (LDA) [75,76], reproduces exactly the total energy of a uniform electron gas at different densities, including long-range van der Waals (vdW) interactions. Some XC functionals, including the PBE functional used here, attempt to address the nonlocal nature of the XC functional in inhomogeneous systems. Other XC functionals, including the vdW-optB86b functional [39,40], attempt to address the inadequate description of long-range dispersive vdW interactions in nonuniform systems. Hybrid functionals adapt a mixture of the PBE functional, with Kohn-Sham eigenvalues that underestimate band gaps, and the Hartree-Fock functional, which overestimates band gaps. Still other functionals try to fit results for a training set of molecules and trust the extrapolation to other systems. No XC functional has been demonstrated to be superior to others in all systems. With so many XC functionals to choose from, this ambiguity raises a semantic question regarding the propriety of attributing the term "*ab initio*" to DFT calculations. In reality, the choice of the XC functional affects binding energies in covalent solids by less than a few percent, and energy differences between different geometries even less. Not only the XC functional but also the numerical DFT implementation including the choice of a basis in codes such as VASP or SIESTA affects the equilibrium bond lengths and binding energies by typically $< 2\%$ in well-converged calculations.

Whereas accurate quantum-chemical WFT calculations are limited to finite-size systems, the quantum Monte Carlo (QMC) approach, also based on wave functions, is a promising tool for infinite systems that eliminates XC functional ambiguities, albeit at a very high computational cost. A QMC study has been performed for a so-called "van der Waals" system, namely, layered black phosphorus [77]. In comparison to QMC results for the weak interlayer interaction, none of the nine XC functionals reproduced correctly the binding energy for both the bulk and the bilayer system. Results for bulk black phosphorus [77] indicate that the DFT-PBE functional underbinds significantly, whereas LDA overbinds. The hybrid vdW-optB86b XC functional seems to work relatively well in that system. For this reason, we compared our DFT-PBE results with those based on vdW-optB86b in Fig. 2(c) for H_2O inside an (8,8) CNT and in Fig. 5(c) for H_2O inside an (8,8) BNNT. We observed that, to some degree, the absolute energy values do depend on the XC functional chosen. On the other hand, changes in the total energy along a trajectory, which correspond to activation barriers affecting flow, are essentially independent of the XC functional. Thus the DFT-PBE approach, which we used for most of this study, appears to be adequate.

We wish to reiterate that most other theoretical approaches describe the interaction of water molecules among themselves and with CNT and BNNT walls using parametrized potentials with an unknown range of validity. In view of this fact, DFT-based studies are expected to provide an unbiased view and guidance to interpret experimental data.

[1] Z. Zhang, X. Huang, Y. Qian, W. Chen, L. Wen, and L. Jiang, Engineering smart nanofluidic systems for artificial ion channels and ion pumps: From single-pore to multichannel membranes, Adv. Mater. (Weinheim) **32**, 1904351 (2020).

[2] W.-Q. Yue, Z. Tan, X.-P. Li, F.-F. Liu, and C. Wang, Micro/nanofluidic technologies for efficient isolation and detection of circulating tumor cells, TrAC, Trends Anal. Chem. **117**, 101 (2019).

[3] S. N. Bhatia and D. E. Ingber, Microfluidic organs-on-chips, Nat. Biotechnol. **32**, 760 (2014).

[4] P. Gravesen, J. Branebjerg, and O. S. Jensen, Microfluidics-a review, J. Micromech. Microeng. **3**, 168 (1993).

[5] G. M. Whitesides, The origins and the future of microfluidics, Nature (London) **442**, 368 (2006).

[6] M. H. Köhler, J. R. Bordin, C. F. de Matos, and M. C. Barbosa, Water in nanotubes: The surface effect, Chem. Eng. Sci. **203**, 54 (2019).

[7] D. Tománek and A. Kyrylchuk, Designing an All-Carbon Membrane for Water Desalination, Phys. Rev. Appl. **12**, 024054 (2019).

[8] Y. Yang, X. Yang, L. Liang, Y. Gao, H. Cheng, X. Li, M. Zou, R. Ma, Q. Yuan, and X. Duan, Large-area graphene-nanomesh/carbon-nanotube hybrid membranes for ionic and molecular nanofiltration, Science **364**, 1057 (2019).

[9] M. H.-O. Rashid and S. F. Ralph, Carbon nanotube membranes: Synthesis, properties, and future filtration applications, Nanomaterials **7**, 99 (2017).

[10] N. G. Chopra, R. J. Luyken, K. Cherrey, V. H. Crespi, M. L. Cohen, S. G. Louie, and A. Zettl, Boron nitride nanotubes, Science **269**, 966 (1995).

[11] S. Faucher, N. Aluru, M. Z. Bazant, D. Blankschtein, A. H. Brozena, J. Cumings, J. Pedro de Souza, M. Elimelech, R. Epsztein, J. T. Fourkas, A. G. Rajan, H. J. Kulik, A. Levy, A.

Majumdar, C. Martin, M. McEldrew, R. P. Misra, A. Noy, T. A. Pham, M. Reed *et al.*, Critical knowledge gaps in mass transport through single-digit nanopores: A review and perspective, J. Phys. Chem. C **123**, 21309 (2019).

[12] A. Kalra, S. Garde, and G. Hummer, Osmotic water transport through carbon nanotube membranes, Proc. Natl. Acad. Sci. USA **100**, 10175 (2003).

[13] F. Zhu and K. Schulten, Water and proton conduction through carbon nanotubes as models for biological channels, Biophys. J. **85**, 236 (2003).

[14] J. A. Thomas and A. J. H. McGaughey, Water flow in Carbon Nanotubes: Transition to Subcontinuum Transport, Phys. Rev. Lett. **102**, 184502 (2009).

[15] G. Hummer, J. C. Rasaiah, and J. P. Noworyta, Water conduction through the hydrophobic channel of a carbon nanotube, Nature (London) **414**, 188 (2001).

[16] R. P. Misra and D. Blankschtein, Insights on the role of many-body polarization effects in the wetting of graphitic surfaces by water, J. Phys. Chem. C **121**, 28166 (2017).

[17] D. J. Mann and M. D. Halls, Water Alignment and Proton Conduction Inside Carbon Nanotubes, Phys. Rev. Lett. **90**, 195503 (2003).

[18] C. Dellago, M. M. Naor, and G. Hummer, Proton Transport through Water-Filled Carbon Nanotubes, Phys. Rev. Lett. **90**, 105902 (2003).

[19] S. Cambré, B. Schoeters, S. Luyckx, E. Goovaerts, and W. Wenseleers, Experimental Observation of Single-File Water Filling of Thin Single-Wall Carbon Nanotubes Down to Chiral index (5,3), Phys. Rev. Lett. **104**, 207401 (2010).

[20] A. I. Kolesnikov, J. M. Zanotti, C. K. Loong, P. Thiyagarajan, A. P. Moravsky, R. O. Loutfy, and C. J. Burnham, Anomalously Soft Dynamics of Water in a Nanotube: A Revelation of Nanoscale Confinement, Phys. Rev. Lett. **93**, 035503 (2004).

[21] Y. Liu, Q. Wang, T. Wu, and L. Zhang, Fluid structure and transport properties of water inside carbon nanotubes, J. Chem. Phys. **123**, 234701 (2005).

[22] K. Koga, G. T. Gao, H. Tanaka, and X. C. Zeng, Formation of ordered ice nanotubes inside carbon nanotubes, Nature (London) **412**, 802 (2001).

[23] G. Cicero, J. C. Grossman, E. Schwegler, F. Gygi, and G. Galli, Water confined in nanotubes and between graphene sheets: A first principle study, J. Am. Chem. Soc. **130**, 1871 (2008).

[24] O. Byl, J. C. Liu, Y. Wang, W. L. Yim, J. K. Johnson, and J. T. Yates, Unusual hydrogen bonding in water-filled carbon nanotubes, J. Am. Chem. Soc. **128**, 12090 (2006).

[25] Y. Maniwa, H. Kataura, M. Abe, A. Udaka, S. Suzuki, Y. Achiba, H. Kira, K. Matsuda, H. Kadowaki, and Y. Okabe, Ordered water inside carbon nanotubes: Formation of pentagonal to octagonal ice-nanotubes, Chem. Phys. Lett. **401**, 534 (2005).

[26] J. K. Holt, Fast mass transport through sub-2-nanometer carbon nanotubes, Science **312**, 1034 (2006).

[27] J. Eijkel, Liquid slip in micro- and nanofluidics: Recent research and its possible implications, Lab Chip **7**, 299 (2007).

[28] E. Lauga, M. Brenner, and H. Stone, Microfluidics: The no-slip boundary condition, in *Springer Handbook of Experimental Fluid Mechanics* (Springer, Berlin, 2007), pp. 1219–1240.

[29] M. Whitby, L. Cagnon, M. Thanou, and N. Quirke, Enhanced fluid flow through nanoscale carbon pipes, Nano Lett. **8**, 2632 (2008).

[30] I. N. Tsimpanogiannis, O. A. Moultos, L. F. Franco, M. B. M. Spera, M. Erdős, and I. G. Economou, Self-diffusion coefficient of bulk and confined water: A critical review of classical molecular simulation studies, Mol. Simul. **45**, 425 (2019).

[31] A. Quandt, A. Kyrylchuk, G. Seifert, and D. Tománek, Liquid Flow through Defective Layered Membranes: A Phenomenological Description, Phys. Rev. Appl. **14**, 044038 (2020).

[32] E. Artacho, E. Anglada, O. Dieguez, J. D. Gale, A. Garcia, J. Junquera, R. M. Martin, P. Ordejon, J. M. Pruneda, D. Sanchez-Portal, and J. M. Soler, The SIESTA method; developments and applicability, J. Phys.: Condens. Matter **20**, 064208 (2008).

[33] G. Kresse and J. Furthmüller, Efficient iterative schemes for *ab initio* total-energy calculations using a plane-wave basis set, Phys. Rev. B **54**, 11169 (1996).

[34] G. Kresse and J. Hafner, *Ab initio* molecular dynamics for liquid metals, Phys. Rev. B **47**, 558 (1993).

[35] G. Kresse and J. Hafner, *Ab initio* molecular-dynamics simulation of the liquid-metal–amorphous-semiconductor transition in germanium, Phys. Rev. B **49**, 14251 (1994).

[36] G. Kresse and D. Joubert, From ultrasoft pseudopotentials to the projector augmented-wave method, Phys. Rev. B **59**, 1758 (1999).

[37] J. P. Perdew, K. Burke, and M. Ernzerhof, Generalized Gradient Approximation Made Simple, Phys. Rev. Lett. **77**, 3865 (1996).

[38] N. Troullier and J. L. Martins, Efficient pseudopotentials for plane-wave calculations, Phys. Rev. B **43**, 1993 (1991).

[39] J. Klimeš, D. R. Bowler, and A. Michaelides, Chemical accuracy for the van der Waals density functional, J. Phys.: Condens. Matter **22**, 022201 (2009).

[40] J. Klimeš, D. R. Bowler, and A. Michaelides, Van der Waals density functionals applied to solids, Phys. Rev. B **83**, 195131 (2011).

[41] H. J. Monkhorst and J. D. Pack, Special points for Brillouin-zone integrations, Phys. Rev. B **13**, 5188 (1976).

[42] M. Hestenes and E. Stiefel, Methods of conjugate gradients for solving linear systems, J. Res. Natl. Bur. Stand. US **49**, 409 (1952).

[43] A. Ambrosetti and P. L. Silvestrelli, Adsorption of rare-gas atoms and water on graphite and graphene by van der Waals-corrected density functional theory, J. Phys. Chem. C **115**, 3695 (2011).

[44] S. K. Kannam, B. D. Todd, J. S. Hansen, and P. J. Daivis, How fast does water flow in carbon nanotubes? J. Chem. Phys. **138**, 094701 (2013).

[45] K. Falk, F. Sedlmeier, L. Joly, R. R. Netz, and L. Bocquet, Molecular origin of fast water transport in carbon nanotube membranes: Superlubricity versus curvature dependent friction, Nano Lett. **10**, 4067 (2010).

[46] D. W. Boukhvalov, M. I. Katsnelson, and Y. W. Son, Origin of anomalous water permeation through graphene oxide membrane, Nano Lett. **13**, 3930 (2013).

[47] X. Wei and T. Luo, Effects of electrostatic interaction and chirality on the friction coefficient of water flow inside single-walled carbon nanotubes and boron nitride nanotubes, J. Phys. Chem. C **122**, 5131 (2018).

[48] A. Sam, K. Vishnu Prasad, and S. P. Sathian, Water flow in carbon nanotubes: The role of tube chirality, Phys. Chem. Chem. Phys. **21**, 6566 (2019).

[49] W. L. Jorgensen, J. Chandrasekhar, J. D. Madura, R. W. Impey, and M. L. Klein, Comparison of simple potential functions for simulating liquid water, J. Chem. Phys. **79**, 926 (1983).
[50] A. Bondi, van der Waals volumes and radii, J. Phys. Chem. **68**, 441 (1964).
[51] M. Mantina, A. C. Chamberlin, R. Valero, C. J. Cramer, and D. G. Truhlar, Consistent van der Waals radii for the whole main group, J. Phys. Chem. A **113**, 5806 (2009).
[52] C. Y. Won and N. R. Aluru, Water permeation through a subnanometer boron nitride nanotube, J. Am. Chem. Soc. **129**, 2748 (2007).
[53] M. E. Suk, A. V. Raghunathan, and N. R. Aluru, Fast reverse osmosis using boron nitride and carbon nanotubes, Appl. Phys. Lett. **92**, 133120 (2008).
[54] K. Ritos, D. Mattia, F. Calabrò, and J. M. Reese, Flow enhancement in nanotubes of different materials and lengths, J. Chem. Phys. **140**, 014702 (2014).
[55] E. Secchi, S. Marbach, A. Niguès, D. Stein, A. Siria, and L. Bocquet, Massive radius-dependent flow slippage in carbon nanotubes, Nature (London) **537**, 210 (2016).
[56] M. Thomas, B. Corry, and T. A. Hilder, What have we learnt about the mechanisms of rapid water transport, ion rejection and selectivity in nanopores from molecular simulation? Small **10**, 1453 (2014).
[57] T. A. Hilder, D. Gordon, and S.-H. Chung, Salt rejection and water transport through boron nitride nanotubes, Small **5**, 2183 (2009).
[58] T. Hilder, R. Yang, V. Ganesh, D. Gordon, A. Bliznyuk, A. Rendell, and S.-H. Chung, Validity of current force fields for simulations on boron nitride nanotubes, Micro Nano Lett. **5**, 150 (2010).
[59] M. Melillo, F. Zhu, M. A. Snyder, and J. Mittal, Water transport through nanotubes with varying interaction strength between tube wall and water, J. Phys. Chem. Lett. **2**, 2978 (2011).
[60] G. Tocci, L. Joly, and A. Michaelides, Friction of water on graphene and hexagonal boron nitride from *ab initio* methods: Very different slippage despite very similar interface structures, Nano Lett. **14**, 6872 (2014).
[61] L. D. Gelb, K. E. Gubbins, R. Radhakrishnan, and M. Sliwinska-Bartkowiak, Phase separation in confined systems, Rep. Prog. Phys. **62**, 1573 (1999).
[62] J. Czwartos, B. Coasne, K. E. Gubbins, F. R. Hung, and M. Sliwinska-Bartkowiak, Freezing and melting of azeotropic mixtures confined in nanopores: Experiment and molecular simulation, Mol. Phys. **103**, 3103 (2005).
[63] A. Srivastava, O. N. Srivastava, S. Talapatra, R. Vajtai, and P. M. Ajayan, Carbon nanotube filters, Nat. Mater. **3**, 610 (2004).
[64] D. R. Lide, *CRC Handbook of Chemistry and Physics*, 67th ed. (CRC Press, Boca Raton, FL, 1986).
[65] S. Joseph and N. R. Aluru, Why are carbon nanotubes fast transporters of water? Nano Lett. **8**, 452 (2008).
[66] I. Hanasaki and A. Nakatani, Flow structure of water in carbon nanotubes: Poiseuille type or plug-like? J. Chem. Phys. **124**, 144708 (2006).
[67] L. Joly, Capillary filling with giant liquid/solid slip: Dynamics of water uptake by carbon nanotubes, J. Chem. Phys. **135**, 214705 (2011).
[68] A. Sam, S. K. Kannam, R. Hartkamp, and S. P. Sathian, Water flow in carbon nanotubes: The effect of tube flexibility and thermostat, J. Chem. Phys. **146**, 234701 (2017).
[69] J. Tao, X. Song, T. Zhao, S. Zhao, and H. Liu, Confinement effect on water transport in CNT membranes, Chem. Eng. Sci. **192**, 1252 (2018).
[70] D. Jassby, T. Y. Cath, and H. Buisson, The role of nanotechnology in industrial water treatment, Nat. Nanotechnol. **13**, 670 (2018).
[71] V. Albergamo, B. Blankert, E. Cornelissen, B. Hofs, W.-J. Knibbe, W. van der Meer, and P. de Voogt, Removal of polar organic micropollutants by pilot-scale reverse osmosis drinking water treatment, Water Res. **148**, 535 (2018).
[72] J. R. Werber, C. O. Osuji, and M. Elimelech, Materials for next-generation desalination and water purification membranes, Nat. Rev. Mater. **1**, 16018 (2016).
[73] J. R. Werber, A. Deshmukh, and M. Elimelech, The critical need for increased selectivity, not increased water permeability, for desalination membranes, Environ. Sci. Technol. Lett. **3**, 112 (2016).
[74] M. Elimelech and W. A. Phillip, The future of seawater desalination: Energy, technology, and the environment, Science **333**, 712 (2011).
[75] D. M. Ceperley and B. J. Alder, Ground State of the Electron Gas by a Stochastic Method, Phys. Rev. Lett. **45**, 566 (1980).
[76] J. P. Perdew and A. Zunger, Self-interaction correction to density-functional approximations for many-electron systems, Phys. Rev. B **23**, 5048 (1981).
[77] L. Shulenberger, A. D. Baczewski, Z. Zhu, J. Guan, and D. Tomanek, The nature of the interlayer interaction in bulk and few-layer phosphorus, Nano Lett. **15**, 8170 (2015).